Supplemental Materials for "Identifying Spinon Excitations from Dynamic Structure Factor of Spin-$1/2$ Heisenberg Antiferromagnet on the Kagome Lattice"

W. Zhu[1,4], Shou-Shu Gong[2,3], D. N. Sheng[3]

[1]*Westlake Institute of Advanced Study, Westlake University, Hangzhou, China*

[2]*Department of Physics, Beihang University, Beijing, 100191, China*

[3]*Department of Physics and Astronomy, California State University, Northridge, California 91330, USA*

[4]*Theoretical Division, T-4 and CNLS, Los Alamos National Laboratory, Los Alamos, New Mexico 87545, USA**

www.pnas.org/cgi/doi/10.1073/pnas.1807840116

CONTENTS

I. NUMERICAL METHOD

In this section, we introduce the details of our numerical simulations of dynamical properties using density-matrix renormalization group (DMRG) algorithm [1]. We also provide a benchmark on the square lattice Heisenberg model using this dynamical DMRG algorithm. The analysis of the finite-size effects is also included.

A. Density-matrix renormalization group algorithm

We perform the calculations based on high accuracy DMRG on cylindrical geometry with a closed boundary in the y direction and an open boundary in the x direction. We denote L_y and L_x as the numbers of unit cells in the y and x directions, respectively. The typical length of the cylinder is $L_x = 24$ (we also tested the length up to $L_x = 36$ and confirmed the result does not change). Most of the calculations are performed on $L_y = 4$ cylinders. We first perform the finite DMRG procedure and obtain the ground state. After obtaining the ground state, we target the dynamical properties (see below) by sweeping the middle $L_y \times L_y$ unit cells to avoid edge excitations.

Here we would like to point out that, although the whole system on the cylinder does not host

translational symmetry along the x-direction, the ground state in the middle of a long cylinder approximatelly satisfies the translational symmetry (the emergent translational period is determined by the nature of the ground state itself). Due to this reason, we can cut the middle $L_y \times L_y$ system and glue it into a torus (with periodic boundary condition along both x- and y-directions), so that the momentum quantum number can be well defined along both x- and y-directions (within $L_y \times L_y$ unit cells in the middle of the cylinder). This process is used for spin structure factor and spin excitation gap calculations in the DMRG community [2].

The conventional DMRG algorithm only targets the ground state $|0\rangle$. To calculate the dynamical spin structure factor, we apply the dynamical DMRG by targeting the following states together with the ground state when sweeping:

$$\begin{aligned} |S^{\alpha}(\mathbf{Q})\rangle &= \hat{S}^{\alpha}(\mathbf{Q})\,|0\rangle \\ |x^{\alpha}(\omega+i\eta)\rangle &= \tfrac{1}{\omega+i\eta-(\hat{H}-E_0)}\,|S^{\alpha}(\mathbf{Q})\rangle \end{aligned}$$

where $|x(\omega)\rangle$ is usually called a *correction vector* which can be calculated by the conjugate gradient method [3] or other algorithm [4]. With the help of the correction vector, the dynamical spin structure factor can be calculated directly:

$$\mathcal{S}^{\alpha\beta}(\mathbf{Q},\omega) = -\frac{1}{\pi} Im\langle 0|\hat{S}^{\alpha}(\mathbf{Q})\frac{1}{\omega+i\eta-(\hat{H}-E_0)}\hat{S}^{\beta}(\mathbf{Q})|0\rangle = -\frac{1}{\pi} Im\langle S^{\alpha}(\mathbf{Q})|x^{\beta}(\omega+i\eta)\rangle \quad (1)$$

where η takes a small positive value as the smearing energy, $\hat{H}$ is the Hamiltonian and E_0 is the ground state energy. Taking these states ($|0\rangle$,$|S^{\alpha}(\mathbf{Q})\rangle$ and $|x^{\alpha}(\omega+i\eta)\rangle$) as target states and optimizing the DMRG basis, allow for a precise calculation of the structure factor for a given frequency ω and a broadening factor η. In this work, all calculations are performed using $\eta = 0.05$ and $\eta = 0.1$ (in units of nearest-neighbor coupling J_1). Since we have to target multi-states in the DMRG process, the truncation error is basically larger than the ground state DMRG.

Here we also comment on the numerical scheme we used in this paper. In general, there are two main algorithms to target dynamics based on the DMRG algorithm. One is to calculate the dynamical spin structure factor in the frequency regime (as outlined above), the other one is to first calculate the time-evolution of the physical quantities and then obtain the dynamical spin structure factor by Fourier transformation. In general, the first method is more accurate in the low-frequency regime, while the second method works better in the high-frequency regime (because the accumulated errors grow as time steps increase in time-dependent DMRG). Based on this reason, in the discussion of low-energy physics of the kagome Heisenberg model, we utilize the first method (Ref. [3, 4]) in this paper.

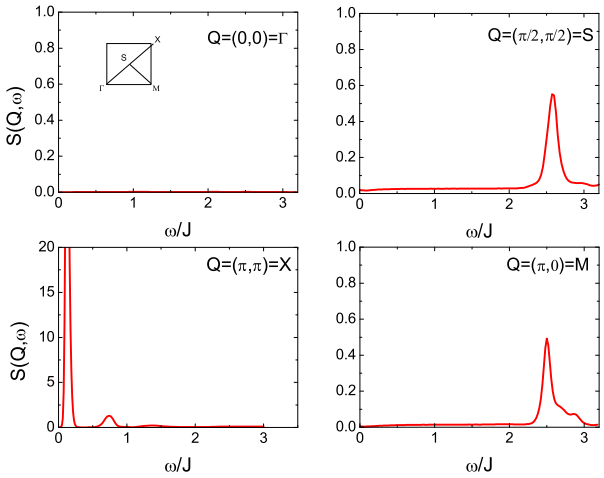

FIG. 1. The energy scan of the dynamical spin structural factor $\mathcal{S}(Q,\omega)$ for the Heisenberg model on the square lattice, for several typical momentum points in BZ. The calculations are performed on a $L_x \times L_y = 24 \times 8$ cylinder by keeping $M = 800$ states.

B. Benchmark on the square lattice

In this section, as a benchmark of our DMRG method, we show the dynamical spin structure factor of the $S = 1/2$ antiferromagnetic Heisenberg model on the square lattice. For the J_1 Heisenberg model on the square lattice, the ground state is a $q = (\pi, \pi)$ Néel ordered state. Thus, we expect to see a single-mode excitation dispersion related to magnon quasiparticles in the dynamical spin structure factor. Fig. 1 shows the energy-dependence of the dynamical spin structure factor $\mathcal{S}(\mathbf{Q},\omega)$ at several typical momenta. As we see, the dynamical spin structure factor at a given momenta is dominated by an individual peak, which indicates a well-defined magnon quasiparticle. We further extract the peak position at each momentum point and plot the single magnon dispersion in Fig. 2, which is largely in agreement with spin wave theory (for $q = (\pi, \pi)$ Néel order, it is believed that spin wave theory can capture the main features of the dynamics except at the $\mathbf{Q} = M$ point.). Interestingly, the $\mathcal{S}(\mathbf{Q} = M, \omega)$ shows an anomalous tail in the high energy regime, which could be attributed to the fact that magnon-magnon interactions are enhanced near $\mathbf{Q} = M$. In Fig. 2, we also compare our results with the large-scale Quantum Monte Carlo (QMC) calculations (red dots) [5]. Around the magnetic vector $X = (\pi, \pi)$, we got consistent results with the QMC, despite we have fewer points due to the limited system size in DMRG. We also notice a difference around $\mathbf{Q} = M = (\pi, 0)$. The main reason for this discrepancy is, our

system size ($L = 8$) is much smaller than that of QMC calculation $L = 48$. Taken as a whole, through this benchmark on the square lattice and extensive tests on one dimensional chains, we conclude that the current scheme can obtain reliable dynamical properties efficiently. In the main text, we will apply the above strategy to the antiferromagnetic Heisenberg model on the Kagome lattice. (Please note that, for Heisenberg model on the square lattice with only nearest-neighbor couplings, the solution of ground state and excited states are available by the QMC calculation. For the Kagome lattice discussed in the main text, it is out of reach using the QMC because of the geometric frustration.)

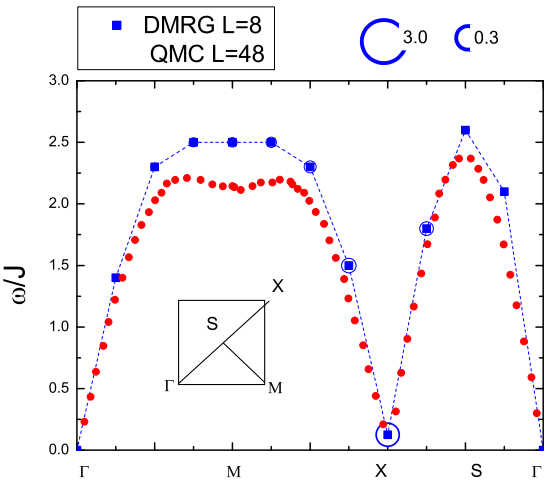

FIG. 2. The peak position (blue dots) of the dynamical structure factors along a path of highly symmetric points in the Brillouin zone. The size of each blue circle is proportional to the static spin structure factor by summing up the dynamical spin structure factor over energy. The red dots are from quantum Monte Carlo simulations [5]

C. Analysis of the finite-size effect

In this work, we utilize the DMRG algorithm to simulate the dynamical response. Although we can easily go beyond the exact diagonalization limit, the DMRG calculation still suffers from the finite-size effect, which will be discussed in detail here.

Since the cylindrical geometry is preferred in the DMRG algorithm, the available lattice system sizes are limited by the width along the wrapped direction similar to the ground state DMRG (saying, L_y, which accounts for the number of unit cells in the wrapped direction). On the Kagome

lattice, the current computational ability is limited to accessing L_y up to 6, depending on the nature of different phases. To be specific, the largest system size is $L_y = 6$ for the Néel $q = (0, 0)$ order and the chiral spin liquid. While for the quantum spin liquid (the KSL) the largest available system is $L_y = 4$, because the highly frustrated nature in the Heisenberg model with only nearest neighbor exchange couplings leads to the slow convergence in DMRG calculations.

We have extensively checked that, the main features of the dynamical spin structure factor are robust for the Néel $q = (0, 0)$ phase and the chiral spin liquid phase, by tuning the system sizes $L_y = 4, 5, 6$. Thus, we have confidence that the nature of the dynamical responses of these two phases shown in the main text are intrinsic properties of the corresponding two-dimensional systems.

Nevertheless, for the quantum spin liquid phase (the KSL), we cannot fully rule out finite-size effects based on a $L_y = 4$ system, since $L_y = 4$ is the only available system size. (We cannot reach a converged ground state in dynamical DMRG algorithm for $L_y = 5, 6$ for the quantum spin liquid phase due to the difficulty to converge in such a state). In the main text, we utilize the twisted boundary condition to inspect the gapless nature on a given finite-size system. The main physical reason is further clarified here. First, tuning the boundary condition is a general method to detect the nature of the ground state on finite-size calculations. Since the available discrete momentum vectors are limited due to the finite-size effect, tuning the twisted boundary condition allows us to reach more momentum points in the Brilliuin zone. Second, for ground states with intrinsic topological orders, it is expected that the ground state manifold is robust to the twisted boundary condition, without energy level crossing. In contrast, energy level crossings may occur by tuning the boundary conditions if the ground state is gapless. Here the picture is akin to Thouless's picture of localization: The energy spectral flow of insulators is robust against boundary conditions, however, energy flow of a metallic phase is not. For a gapless phase, the change of the energy spectrum by twisted boundary conditions inevitably leads to substantial difference in the dynamical response functions. Based on these reasons, we inspect the dynamical response for the quantum spin liquid phase by tuning different boundary conditions. This is a way out for uncovering the intrinsic nature of the ground state using finite-size calculations, although it is not conclusive.

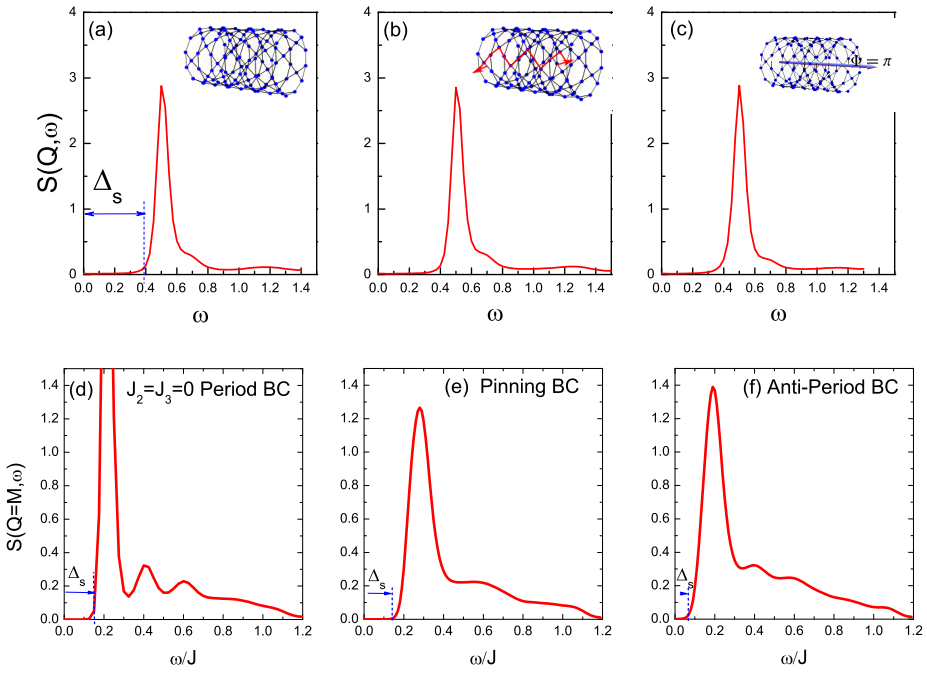

FIG. 3. DSSF for CSL phase (a-c) and KSL phase (d-f) for different boundary conditions (BCs): (a,d) periodic BC in wrapped direction (b,e) periodic BC on wrapped direction and a pinning field on the open direction, and (c,f) anti-periodic BC in the wrapped direction.

D. Tuning boundary conditions

We address the question of whether or not the ground state of the Kagome spin liquid is gapped, which holds the clue to distinguish the different theoretical scenarios [6, 7], by inspecting the response of the system under different boundary conditions. As a benchmark, we first test the system in the gapped CSL phase. Since the CSL is equivalent to the $\nu = 1/2$ bosonic Laughlin state [8], the system has two-fold topological degenerate ground states. In the DMRG simulation, the ground state in the spinon sector can be obtained by adiabatically changing the boundary condition by a 2π phase. As shown in Fig. 3(a-b), the dynamic structure factor of the two ground states are almost identical, which can be understood by the fact that local measurements are unable to distinguish different topologically degenerate ground states.

Now we inspect the response of the Kagome spin liquid. Fig. 3(d) shows $\mathcal{S}(\mathbf{Q} = M, \omega)$, by imposing periodic boundary condition on the wrapped direction. As a comparison, Fig. 3(e) shows the case of additionally pinning a spinon at each open end of the cylinder. Although the spin gap remains robust, the predominant spectral peak in the low-energy regime becomes broader.

Moreover, by imposing an anti-periodic boundary condition in the wrapped direction, as shown in Fig. 3(f), the excitation gap Δ_s shrinks from $\Delta_s \approx 0.16$ to a smaller value ≈ 0.075, signaling that the spin excitation gap is sensitive to the boundary condition. Here, the dramatic change of spectral lineshape and the shrinking of the spin gap in the DSSF, indicate that the ground state may not have a robust spin gap. Of course, the finite size effect is generally important, which calls for future work to perform a finite-size scaling analysis.

As we see here, for Kagome Heisenberg antiferromagnetic model with only nearest-neighbor couplings ($J_2 = J_3 = 0$), a small spin gap holds even when we check the different boundary conditions. This result is consistent with the existing literatures by calculating the spin excitation gap directly [9, 10]. Moreover, we also study the Kagome Heisenberg antiferromagnetic model by adding a DM interaction term (see main text and SI Appendix IV). In the presence of DM interaction, we get the similar feature of the dynamic spin structure factor. That is, The dynamic spectral changes by tuning boundary conditions, which is in striking contrast to the expectation of gapped spin liquid (e.g. chiral spin liquid).

To sum up, although caution is needed when making a statement about the thermodynamic limit, by tuning boundary conditions we find some evidences on the system sizes that we can access, which supports the kagome spin liquid is not a gapped one.

II. STATIC SPIN STRUCTURE FACTOR

The static spin structure factor shown in the main text is calculated using the same setup for calculation of dynamic spin structure factor. That is, we first perform the DMRG procedure and obtain the ground state. After we obtain the ground state, we calculate static spin structure factor using the correlation functions defined in the central $L_y \times L_y$ unit cells of the cylinder, based on the definition of Eq. 2 (main text).

Since the static and dynamic structure factors are calculated in the same condition, we can directly compare the static structure factor obtained from two different methods: 1) We calculate static spin structure factor using the static correlation function $\mathcal{S}(\mathbf{Q}) = \langle \mathbf{S}(-\mathbf{Q}) \cdot \mathbf{S}(\mathbf{Q}) \rangle = \frac{1}{N} \sum_{i,j} e^{i\mathbf{Q}\cdot(\mathbf{r}_i - \mathbf{r}_j)} \langle \mathbf{S}_i \cdot \mathbf{S}_j \rangle$; 2) We obtain the static spin structure factor through dynamical spin structure factor by summing over the frequency: $\mathcal{S}(\mathbf{Q}) = \int_0^\infty d\omega \mathcal{S}(\mathbf{Q}, \omega)$. As shown in Fig. 4, we present the static spin structure factor obtained by these two methods. Here we use $q = (0, 0)$ phase as an example. We see that the results obtained using different methods are consistent with

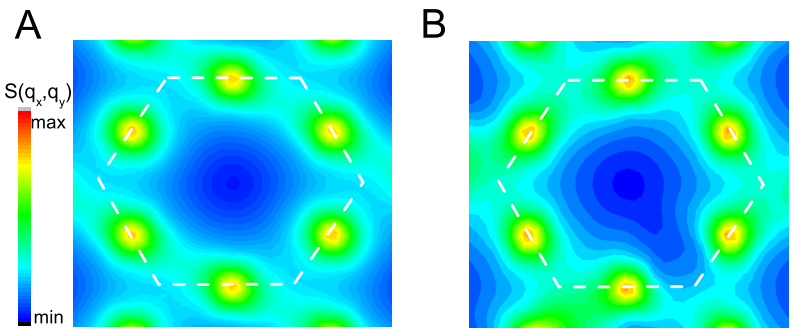

FIG. 4. Comparison of static spin structure factor from two different methods: (A) the results obtained by correlation functions and (B) the results by summing the dynamic structure factor over frequency ($\mathcal{S}(\mathbf{Q}) = \int_0^\infty d\omega \mathcal{S}(\mathbf{Q},\omega)$). Here we use $q = (0,0)$ phase as an example. The calculation is performed on $L_y = 4$ cylinder.

each other, e.g. peak structure around $\mathbf{Q} = M$. It is observed a small anisotropy in figure B, which is due to correlation function is not exactly the same along x and y direction on the cylinder geometry. Moreover, this comparison serves as additional tests of the method for obtaining dynamic spin structure factor.

III. TRANSITION FROM CHIRAL SPIN LIQUID PHASE TO NÉEL $q = (0,0)$ PHASE

In this section, we discuss the phase transition from the chiral spin liquid phase to the magnetic Néel $q = (0,0)$ phase. This phase transition is interesting due to the following reasons. First, it is intriguing to understand the low-energy peak structure in the dynamical spin structure factor at the $\mathbf{Q} = M$ point. Second, it is an exotic example of a continuous phase transition between a gapped topologically ordered state and a topologically trivial state.

According to the global phase diagram in the main text (Fig. 1(A)), for finite $J_2 > 0.15$ different phases may appear depending on J_3. Tuning J_3 will drive a phase transition from the chiral spin liquid phase to the magnetic $q = (0,0)$ phase. It has been found that, the chiral spin liquid undergoes a *continuous* phase transition to a Néel $q = (0,0)$ phase [11], as evidenced by the fact that all local order parameters change smoothly across the phase transition point. However, the reason for this continuous phase transition is less understood, because the transition between a gapped topologically ordered phase and a topologically trivial phase is often thought to be first-

order.

We show the evolution of dynamical spin structure factor for various J_3, by setting $J_2 = 0.2J_1$. We focus on momentum wave vector $\mathbf{Q} = M$ in this section. As shown in Fig. 3 (main text), the evolution of dynamical spin structure factor at momentum $\mathbf{Q} = M$ for various J_3 shows some key features: By approaching the transition point, in the chiral spin liquid phase ($J_3 > 0.15J_1$), the lowest energy peak at the $\mathbf{Q} = M$ point moves towards the low-frequency regime, and the peak intensity gradually increases. Based on the above observations, a natural interpretation of the peak structure in the chiral spin liquid phase is a two-spinon resonance state. The reason is that low-energy excitations in the Néel phase should be the magnon quasiparticle, which can be viewed as a bound state of two spinons. Taking into account that the elementary excitation in the chiral spin liquid phase is a *deconfined* spinon [12], we can take the peak in the chiral spin liquid as a two-spinon resonance state, while the peak in Néel phase is a two-spinon bound state (equivalent to a magnon state). A two-spinon resonance state naturally depends on the interaction coupling J_3. By approaching the critical point, the two-spinon resonance moves towards zero frequency. At the critical point, the two-spinon resonance state becomes a two-spinon bound state (equivalent to a magnon). The further condensation of pairs of spinons should lead to the formation of Néel magnetic order. In other words, this picture leads to two important physical insights: First, the peak of the dynamical spin structure factor at momentum $\mathbf{Q} = M$ in the chiral spin liquid can be interpreted as a two-spinon resonance state. Second, the transition from chiral spin liquid to a Neel phase can be understood as the formation of a condensate of two-spinon bound states or magnons. It therefore provides a microscopic understanding of continuous phase transition between the chiral spin liquid and the Neel phase.

In the above analysis, the peak structure in the dynamic spin structure factor of the Neel phase and the chiral spin liquid occur at the same momentum point ($\mathbf{Q} = M$), which makes the mechanism of spinon pair condensation possible. If the magnetic wave vector of the underlying long-range magnetic order is different from that of two-spinon resonance state in the spin liquid, the phase transition from chiral spin liquid to magnetically ordered phase should be first order. For example, the transition from chiral spin liquid to cuboc1 phase in the global phase diagram is first-order [11]. To sum up, the evolution of the dynamical spin structure factor across the critical point, is intuitive to understand the nature of the ground state properties, and provides invaluable insights on the nature of related phase transitions.

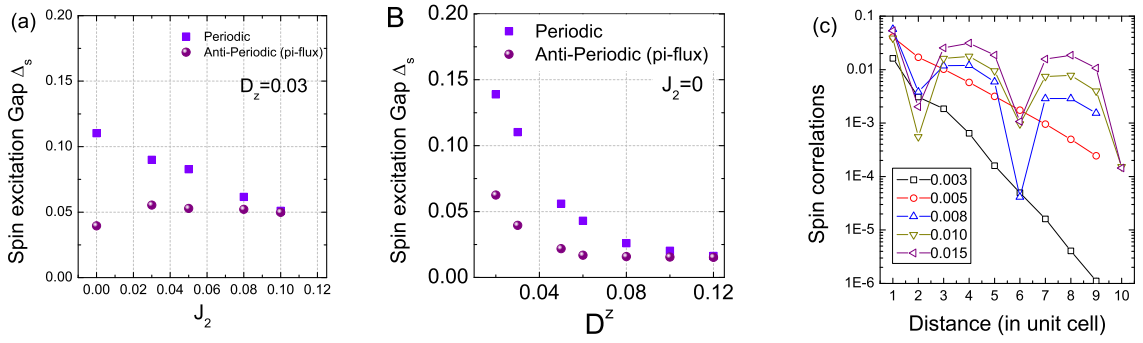

FIG. 5. (a) Spin excitation gap as a function of J_2 by setting $D^z = 0.03$ and (b) spin excitation gap as a function of D^z by setting $J_2 = 0$. The spin excitation gap is defined by the energy difference between the lowest state in $S_z^{tot} = 1$ and $S_z^{tot} = 0$: $\Delta_s = E_0(S_z^{tot} = 1) - E_0(S_z^{tot} = 0)$, where the lowest energy state of $S_z^{tot} = 1$ is computed by targeting $S_z^{tot} = 1$ in the center of the cylinder based on the ground state in $S_z^{tot} = 0$ [2, 9]. (c) spin correlations $\langle S_i^+ S_{i+d}^- \rangle$ for various D^z, by setting $J_2 = 0.0$. These results are obtained on a $L_y = 4$ cylinder.

IV. SPIN CORRELATIONS AND SPIN GAP IN THE PRESENCE OF DM INTERACTION

In the main text, we show a phase diagram of Kagome antiferromagnetic Heisenberg model as a function of out-of-plane DM interaction D^z and next-nearest-neighbor coupling J_2. (We only consider out-of-plane DM interaction because it is around one order of magnitude larger than the in-plane component according to experimental estimates.) The phase boundary between spin liquid phase and magnetic $q = (0, 0)$ phase is determined by the spin excitation gap and spin correlations. In Fig. 5(a-b), we show the spin excitation gap (defined by $\Delta_s = E_0(S_z^{tot} = 1) - E_0(S_z^{tot} = 0)$) dependence on parameter J_2 and D^z, respectively. It is found that the spin excitation gap decreases monotonically approaching the phase boundary. In particular, in the spin liquid phase, the spin excitation gap strongly depends on the twisted boundary condition, indicating the finite spin excitation gap may be due to finite-size effects. In contrast, in the magnetically ordered phase, the spin excitation gap has little dependence on the twisted boundary condition. As shown in Fig. 5(c), the spin correlation $\langle S_i^+ S_{i+d}^- \rangle$ provides another evidence for the phase boundary. The spin correlation exponentially decays with the distance, for $D^z < 0.08$ and $J_2 = 0.0$. For $D^z \geq 0.08$, the long-ranged order emerges as the spin correlation tends to saturate to a finite value at large distance. Based on these facts, we determine $D^z \approx 0.08$ as the phase boundary at $J_2 = 0.0$, which is largely consistent with the previous estimation from an ED calculation [13].

Using the similar method, we determine the phase boundary for the non-zero J_2 case, and map out the full phase diagram as shown in the main text.

At last, we show the dynamic spin structure factor in kagome spin liquid phase with and without DM interactions. In the kagome spin liquid phase, the dynamic spin structure factor stays similar to the one without the DM interactions (when we apply the periodic boundary condition along y-direction). As shown in Fig. 6, we compare the $\mathcal{S}(\mathbf{Q},\omega)$ at $D^z = 0$ and $D^z = 0.06$. The two results are qualitatively similar, with a spectral intensity predominantly in the low frequency region, and a broad spectral distribution in the high frequency region.

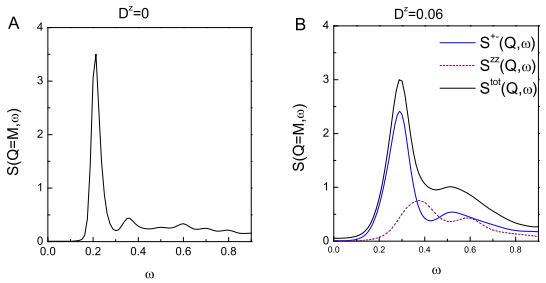

FIG. 6. Dynamic spin structure factor of the Kagome spin liquid phase without DM interaction (A) $D^z = 0.0$ and (B) with DM interaction $D^z = 0.06$. When we consider a non-zero DM interaction (B), the spin rotation symmetry is broken thus we include transverse mode $\mathcal{S}^{+-}$ (blue solid) and longitudinal mode $\mathcal{S}^{zz}$ (purple dashed). The black solid line is the total spin structure factor.

* phwzhu@gmail.com; donna.sheng1@csun.edu

[1] S. R. White, Phys. Rev. Lett. **69**, 2863 (1992).

[2] E. M. Stoudenmire and S. R. White, Annual Review of Condensed Matter Physics **3**, 111 (2012).

[3] T. D. Kühner and S. R. White, Phys. Rev. B **60**, 335 (1999).

[4] E. Jeckelmann, Phys. Rev. B **66**, 045114 (2002).

[5] H. Shao, Y. Q. Qin, S. Capponi, S. Chesi, Z. Y. Meng, and A. W. Sandvik, Phys. Rev. X **7**, 041072 (2017).

[6] Y. Ran, M. Hermele, P. A. Lee, and X.-G. Wen, Phys. Rev. Lett. **98**, 117205 (2007).

[7] M. B. Hastings, Phys. Rev. B **63**, 014413 (2000).

[8] R. B. Laughlin, Phys. Rev. Lett. **50**, 1395 (1983).

[9] S. Yan, D. A. Huse, and S. R. White, Science **332**, 1173 (2011).

[10] Y.-C. He, M. P. Zaletel, M. Oshikawa, and F. Pollmann, Phys. Rev. X **7**, 031020 (2017).

[11] S.-S. Gong, W. Zhu, L. Balents, and D. N. Sheng, Phys. Rev. B **91**, 075112 (2015).

[12] S.-S. Gong, W. Zhu, and D. Sheng, Scientific reports **4**, 6317 (2014).

[13] L. Messio, O. Cépas, and C. Lhuillier, Phys. Rev. B **81**, 064428 (2010).